Submitted to the Special Issue on Advances in Fatigue and Fracture celebrating the 40th anniversary of FFEMS

March 2019

Lifetime estimation of mechanical assemblies under constant amplitude fretting fatigue loading

Andrea Carpinteri, Sabrina Vantadori, Andrea Zanichelli

Department of Engineering & Architecture, University of Parma, Parco Area delle Scienze 181/A, 43124 Parma, Italy

Corresponding Author: Andrea Carpinteri, andrea.carpinteri@unipr.it

ABSTRACT

In the present paper, a new analytical methodology to estimate both crack path and lifetime of metallic structural components under fretting fatigue elastic partial slip loading condition is proposed. Such a methodology consists in the joint application of (i) the criterion by Carpinteri et al. for metallic structures under multiaxial constant amplitude fatigue loading in high-cycle fatigue regime, (ii) the critical direction method by Araújo et al., and (iii) the critical distance method by Taylor, in the form of the Line Method. The accuracy of the above methodology is evaluated through experimental tests available in the literature, performed employing two cylindrical fretting pads pressed with a constant normal load against a dog-bone type test specimen subjected to a cyclic axial load. All these components are made of Al 7075-T651 aluminium alloy.

KEYWORDS: Aluminium alloy, Crack path, Critical distance, Critical plane approach, Fretting fatigue, Lifetime assessment

NOMENCLATURE

a	theoretical Hertzian contact semi-width
C_a	amplitude of the shear stress component lying on the critical plane
E	Young modulus
L	El-Haddad intrinsic crack length
m	slope of the S-N curve under fully reversed normal stress
m^*	slope of the S-N curve under fully reversed shear stress
N_a	amplitude of the normal stress component perpendicular to the critical plane
$N_{eq,a}$	equivalent normal stress amplitude
$N_{f,cal}$	calculated fretting fatigue life
$N_{f,exp}$	experimental fretting fatigue life
N_m	mean value of the normal stress component to the critical plane
P	constant normal load (compression)
Q	cyclic tangential load
Q_a	amplitude of tangential load
$\hat{1},\hat{2},\hat{3}$	averaged principal stress directions
δ	off-angle defining the normal to the critical plane
$\sigma_{af,-1}$	material fatigue strength under fully reversed normal stress at N_0 loading cycles
σ_B	cyclic axial stress applied to the specimen
$\sigma_{B,a}$	amplitude of axial stress applied to the specimen

σ_u ultimate tensile strength

σ_y yield strength

$\Delta\sigma_{af}$ fatigue limit range

$\sigma_{\hat{1},\max}$ maximum value of σ_1 during a loading cycle

$\sigma_1, \sigma_2, \sigma_3$ instantaneous principal stresses

θ_{cr} orientation of the critical plane

$\tau_{af,-1}$ material fatigue strength under fully reversed shear stress at N_0 loading cycles

$\Delta K_{I,th}$ threshold stress-intensity factor range

ν Poisson's coefficient

1. INTRODUCTION

Fretting is a contact phenomenon that may occur between two mating surfaces subjected to cyclic relative motion induced, for example, by extremely small amplitude vibrations. The damage process associated with fretting is caused by the synergistic contribution of wear, corrosion, and crack nucleation and growth **[1-4]**. According to Hurricks **[5]**, a typical damage mechanism can be observed in engineering materials (such as steel and aluminium) subjected to fretting.

The scarring of the superficial oxide layer is the initial mechanism that can be observed **[6]**. Such a mechanism, called *fretting wear*, is responsible for the appearance of micro-debris between the contact surfaces. Consequently, the value of the friction coefficient has experimentally been observed to increase during the first few hundreds of loading cycles **[7-9]**.

As the number of loading cycles increases, plastic deformations take place near the contact surface, thus resulting in possible nucleation of several grain-sized microcracks **[5,7]**. When such microcracks affect the superficial oxide layer, additional micro-debris arise. This mechanism, together with corrosive environmental conditions, accelerates the wear process.

In such a condition, the cyclic loading promotes the propagation of one or more of the aforementioned microcracks into the bulk material, and this phenomenon is called *fretting fatigue*. It should be highlighted that the near-surface nucleation stage is dominated by the high stress gradient due to contact, whereas bulk or global stress mainly affect the propagation stage.

Unlike sliding, fretting fatigue does not concern global relative motion of the contact surfaces since the contact zone consists of both a stick region, where no relative displacements arise, and a slip region at the trailing edges of the contact zone, characterised by micro-slips of the order of 10^{-2} mm **[1]**.

Fretting fatigue has been recognised as a primary failure mode across a wide range of structural components, such as dovetail joints **[10-13]**, bolt and riveted joints **[14-16]**, spline coupling **[13,17]**, running cables and overhead conductors **[18-20]**. Therefore, fretting fatigue has attracted the interest of many researchers, and various aspects of this phenomenon have been investigated during the last decades, such as life prediction, influential factors, mechanisms, new fretting test set-ups, possible palliatives **[10,21-26]**.

In particular, many damage models and approaches related to both crack nucleation and propagation phase have been applied to assess the fatigue life of fretting affected components. However, since crack nucleation life is around 90% of the total fretting fatigue life for all kinds of tests **[27]**, damage models concerning the crack nucleation phase are mainly employed in fretting fatigue assessment. Such models have recently been classified by Bhatti and Wahab **[28]** on the basis of the approach used to define failure. In more detail, four different approaches have been distinguished: critical plane (CP) approach, stress invariant (SI) approach, fretting specific parameters (FSP) approach, and continuum damage mechanics (CDM) approach.

According to the critical plane approach, fatigue assessment is performed on a specific plane named critical plane, which is prone to be the crack nucleation plane. This approach can further be classified as stress-based, strain-based, or strain energy density-based. Findley et al. **[29]** and later McDiarmid **[30]** proposed two different stress-based parameters for high-cycle fatigue regime, both of them depending on the maximum normal stress. Brown and Miller **[31]** suggested a strain-based evaluation of fatigue life, based on a linear combination of shear strain amplitude and maximum normal strain range. Fatemi and Socie **[32]** modified the Brown and Miller parameter by substituting the normal strain with the normal stress, in order to include the effect of non-proportional loading and mean stress. Moreover, among strain energy density-based parameters, the one by Smith et al. **[33]**, known as the Smith Watson and Topper (SWT) parameter (defined as maximum tensile stress

multiplied by strain amplitude) and the one by Liu **[34]** (based on virtual strain energy) are the most widespread.

Stress invariant approach is similar to stress-based CP approach. For instance, the parameter suggested by Crossland **[35]** takes into account both the maximum amplitude of second invariant of the deviatoric stress tensor and the maximum hydrostatic pressure. With respect to CP models, this model is characterised by a less time-requesting computation, but it does not give us information on the crack orientation.

In order to take into account the high frictional forces at the contact interface, fretting specific parameters incorporating the effect of slip amplitude have been proposed. Ruiz et al. **[36]** combined relative slip amplitude with shear stress to obtain the frictional energy due to contact forces, and later added tensile stress to such a frictional energy for better predicting the actual crack location. Ding et al. **[37]** modified the SWT parameter including the effect of frictional work, in order to take into account the fretting wear phenomenon.

Continuum damage mechanics approach aims to describe the nucleation process inside a representative volume element at mesoscale, by employing mechanical variables **[38]**. More precisely, a damage scalar variable incorporating the effect of mean stress, stress amplitude, loading history, material and loading conditions is adopted. Different CDM models are available in the literature, such as those proposed by Bhattiacharya and Ellingwood **[39]**, Chaboche **[40]**, and Lemaitre et al. **[41]**, which assume that the crack nucleation occurs when a critical value of damage is

achieved. Since damage is computed as a scalar variable, no information can be obtained about crack orientation.

In the present paper, a new methodology falling in the category of the stress-based critical-plane approach is discussed to evaluate the initial crack path and the lifetime of metallic structures under fretting fatigue elastic partial slip loading condition. Experimental tests carried out by Vázquez et al. **[26,42]** on Al 7075-T651 dog-bone specimens are described in Section 2. Such experimental tests are used to validate the proposed methodology, which derives from the joint application of (i) the multiaxial fatigue criterion by Carpinteri et al. (to evaluate the fatigue life **[43-45]**), (ii) the critical direction method by Araújo et al. and (iii) the critical distance method by Taylor (to define the critical plane **[46,47]**), each of them being outlined in Section 3. Then, the proposed methodology based on the above criterion and methods is described in Section 4, and the results obtained are discussed in Section 5. Finally, conclusions are summarised in Section 6.

The present paper attempts to estimate both crack path and lifetime of metallic structural components under fretting fatigue elastic partial slip loading condition, by using the above novel methodology based on a multiaxial fatigue method previously developed for fatigue assessment of smooth, notched and welded components characterised by high-cycle fatigue regime **[43-45]**. Being based on linear-elastic stresses, such a methodology could be easily applied to practical situations in the industrial field.

2. EXPERIMENTAL CAMPAIGN

The experimental tests examined in the present paper were carried out at the University of Seville **[26,42]** using a typical cylinder-to-flat contact configuration. Two cylindrical pads were pressed against a dog-bone specimen through a constant normal load P (compression). Further, a cyclic axial load was applied to the specimen at a frequency equal to $10Hz$, and it led to a bulk stress σ_B in the specimen. Moreover, the two pads experienced a cyclic tangential load Q, that generated a time-varying distribution of shear stress at the contact interfaces. Note that σ_B and Q were in phase with each other, both of them characterised by loading ratio $R=-1$.

The middle cross-sectional area of the specimen had a prismatic shape, where $t=7mm$, $W=10mm$ and $l=165mm$ were the thickness, the width, and the length of the specimen, respectively (**Figure 1**). The radius of the pads, R, was equal to $100mm$. Both specimen and cylindrical pads were made of Al 7075-T651 aluminium alloy, whose mechanical properties are listed in **Table 1 [48]**.

Figure 1.

Table 1.

Three different fretting fatigue loading configurations are hereafter analysed. The fretting loads and the values of the experimental fatigue life $N_{f,exp}$ are listed in **Table 2 [42]** for each

test examined. Note that the compression P has the same value for all the tests. Therefore, according to the Hertzian theory, the theoretical contact width can be computed as follows:

$$2a = \sqrt{\frac{16PR}{\pi E^*}} \quad \textbf{(1)}$$

being E^* the Young's modulus for plane strain condition:

$$E^* = \frac{E}{2\left(1-\nu^2\right)} \quad \textbf{(2)}$$

Table 2.

A confocal microscope was used to analyse the crack profile. Details are available in Ref. **[26]**.

The crack paths are plotted in **Figure 2 [49]**, for tests Nos 1, 3 and 5. More than one crack may be observed on the same fracture surface: three semi-elliptical cracks were recognised for test No.1, two for test No.3 and one for test No.5. Such cracks grew almost perpendicular to the contact surface or outside the contact zone for the first microns in depth. Then all cracks turned towards the contact zone.

The crack paths, up to a normalised depth equal to 0.06, can be described by means of an average inclination angle measured from the line perpendicular to the contact surface. The values of this angle are equal to 20°, 16° and 12° for tests No.1, No.3 and No.5, respectively.

Figure 2.

3. OUTLINE OF THE CRITERION AND METHODS EMPLOYED

The results of the experimental campaign described in Section 2 have been used to validate the proposed analytical methodology.

Under fretting fatigue elastic partial slip loading condition, the stress field in the vicinity of the contact zone is evaluated by using both the closed-form solution by Johnson **[50]** (based on the formalisms by Hertz **[51]**, Cattaneo and Mindlin **[52,53]**, McEven **[54]**) and the closed-form solution by Nowell and Hills **[55]**. Details on such solutions can be found in Ref.**[56]**.

3.1 The Carpinteri et al. criterion

The fatigue life evaluation can be performed by employing the Carpinteri et al. criterion **[43-45]**, which belongs to the category of the critical plane-based criteria. It is formulated in terms of stress when the high-cycle fatigue regime occurs.

The fatigue life is evaluated by employing an equivalent stress amplitude obtained after reduction of the multiaxial stress state to an equivalent uniaxial one. The main steps of the above criterion are hereafter summarised.

Firstly, the critical plane is determined. In particular, the principal Euler angles to identify the time-varying principal stress directions $1,2,3$ at the material point being analysed are averaged by means of a weight function, $W(t)$ **[43]**. Such a function works so that the averaged principal Euler angles and, consequently, the averaged principal stress directions $\hat{1},\hat{2},\hat{3}$

correspond to those at the time instant when the maximum principal stress σ_1 attains its peak value within a loading cycle. Then, the critical plane orientation is linked to the averaged maximum principal stress direction $\hat{1}$ through the off-angle δ:

$$\delta = \frac{3\pi}{8}\left[1-\left(\frac{\tau_{af,-1}}{\sigma_{af,-1}}\right)^2\right] \quad \textbf{(3)}$$

where $\tau_{af,-1}$ and $\sigma_{af,-1}$ are the material fatigue strength under fully reversed shear stress and that under fully reversed normal stress, respectively, at the reference number N_0 of loading cycles. Note that, according to the Carpinteri et al. criterion, the critical plane is assumed to coincide with the dominant failure plane.

The second step concerns the computation of the stress components acting on the critical plane. Note that the normal stress component perpendicular to the critical plane is characterized by a fixed direction with respect to time and, therefore, both the mean value N_m and the amplitude N_a are easily evaluated. On the other hand, since the shear stress component lying on the critical plane has a time-varying direction, the amplitude C_a is computed by means of the Maximum Rectangular Hull method proposed by Araújo et al. **[57]**.

Finally, an equivalent normal stress amplitude $N_{eq,a}$ is employed to evaluate the finite life fatigue strength. In particular, the number of loading cycles to failure, $N_{f,cal}$, can be obtained from the following equation:

$$\sqrt{N_{eq,a}^2+\left(\frac{\sigma_{af,-1}}{\tau_{af,-1}}\right)^2\left(\frac{N_{f,cal}}{N_0}\right)^{2m}\left(\frac{N_0^*}{N_{f,cal}}\right)^{2m^*}C_a^2}=\sigma_{af,-1}\left(\frac{N_{f,cal}}{N_0}\right)^m \quad \textbf{(4)}$$

where m and m^* are the slopes of the S-N curves under fully reversed normal stress and under fully reversed shear stress, respectively, and $N_{eq,a}$ is given by the linear combination between N_a and N_m, proposed by Goodman **[58]**:

$$N_{eq,a}=N_a+\sigma_{af-1}\left(\frac{N_m}{\sigma_u}\right) \quad \textbf{(5)}$$

being σ_u the ultimate tensile strength of the material.

Note that Eq.(5) takes into account the strength decrease due to the simultaneous presence of a tensile mean normal stress and an alternating normal stress. Therefore, N_m should be conservatively assumed to be equal to zero when it is a compressive stress.

3.2 The critical direction method by Araújo et al.

The critical direction method by Araújo et al. **[46]** is here employed to determine the orientation of the critical plane.

As is well-known, according to the critical plane-based approaches, the critical plane is determined by employing the multiaxial stress state at a single material point. However, in the case of high stress gradient, the critical planes related to adjacent material points may be characterised by different orientations due to the variety of stress state in the process zone. From a mechanical point of view, the crack initiation direction in a high stress gradient zone does not depend on the

stress state in a single point only, but it is controlled by an average stress condition within a given material volume **[59]**.

Araújo et al. **[46]** proposed the critical direction method in order to identify the critical plane in the case of high stress gradient zones, that is, the case of fretting fatigue configurations. In such a condition, the critical plane orientation is determined by maximising the averaged value of a suitable quantity computed over a process zone.

Such a quantity is here represented by the amplitude of the equivalent normal stress, $N_{eq,a}$, whereas the process zone is represented by planes starting from a point (named hot-spot) on the contact surface, as is discussed in Sub-Section 3.3. The critical plane is the one that maximises the mean value of $N_{eq,a}$ in the process zone.

3.3 The critical distance method by Taylor

Now the critical distance method by Taylor **[47]**, in the form of the Line Method (LM), is employed in order to define the position of the critical point P_{cr} where to perform the fretting fatigue assessment.

Let us consider a point (named Hot-spot, H) on the contact surface ($-a \le x \le a$, **Figure 3**), characterised by the maximum value of the averaged maximum principal stress $\sigma_{\hat{1}}$ computed through the Carpinteri et al. criterion: for the examined configuration, H is found to be located at the trailing edge ($x = +a$). According to the

LM method, a segment with a length equal to twice the El-Haddad intrinsic crack length L

$$L = \frac{1}{\pi}\left(\frac{\Delta K_{I,th}}{\Delta \sigma_{af}}\right)^2 \qquad (6)$$

has to be considered, where $\Delta K_{I,th}$ is the threshold value of the stress-intensity factor range and $\Delta \sigma_{af}$ is the uniaxial fatigue limit range, both referred the same loading ratio.

Figure 3.

In conclusion, the critical point P_{cr} is here assumed to be located at the end of such a segment $2L$, starting from point H and with direction determined by applying the critical direction method outlined in Sub-Section 3.2.

4. DESCRIPTION OF THE PROPOSED METHODOLOGY

Now a description of the proposed methodology for fretting fatigue assessment is provided. The flowchart of such a methodology is shown in **Figure 4**, whereas the main steps are hereafter summarised.

Figure 4.

Three categories of input data need to be set: geometrical sizes, mechanical properties and loading conditions. Regarding the first category, the sizes of both cylindrical pads and specimen are needed: radius of the pads, R, and thickness t and width W of the

specimen. The parameters belonging to the second category are: the elastic modulus E, the Poisson's coefficient ν, the coefficient of friction μ, the ultimate tensile strength σ_u, the fatigue limits under fully reversed normal and shear stress, $\sigma_{af,-1}$ and $\tau_{af,-1}$, respectively, the slopes of the S-N curves under fully reversed normal and shear stress, m and m^*, respectively, and the threshold stress-intensity factor range $\Delta K_{I,th}$. The loading conditions to be set are compression P, amplitude Q_a of the cyclic tangential load, and both amplitude $\sigma_{B,a}$ and mean stress $\sigma_{B,m}$ of the tensile cyclic stress applied to the specimen.

Let us take into account the configuration shown in **Figure 3**. According to the critical direction method, in the form of the Line Method (LM), material planes having length equal to $2L$, starting from the hot-spot H and characterised by different orientations (i.e. different values of θ, see **Figure 3**), are examined in order to determine the orientation of the critical plane.

Firstly, the El-Haddad intrinsic length L is computed by means of Eq.(6). Then, a suitable value of the angular increment, $\Delta\theta$, needs to be set: in the present work, $\Delta\theta = 1°$ is taken. The procedure starts by analysing the initial value $\theta = 0°$. The values of $N_{eq,a}(\theta, r)$ acting on the corresponding plane are computed in equally spaced points belonging to the segment having length $2L$ starting from the hot-spot H, with direction defined by angle θ.

Note that the above segment is the two-dimensional representation of the critical plane. The values of equivalent

normal stress amplitude are computed by considering the critical plane orientation as fixed (equal to θ). This means that the procedure discussed in Section 3.1 to determine the critical plane orientation through the off-angle δ is not employed here. Subsequently, the average value $\overline{N}_{eq,a}(\theta)$ is obtained from the following equation:

$$\overline{N}_{eq,a}(\theta) = \frac{1}{2L}\int_0^{2L} N_{eq,a}(\theta, r)\, dr \tag{7}$$

Then, a new material plane is taken into account by updating the value of the angle, $\theta = \theta + \Delta\theta$. Such a procedure is iterated for all the material planes belonging to the specimen half-space, that means until θ is equal to $180°$.

The orientation of the material plane that produces the maximum value of $\overline{N}_{eq,a}(\theta)$ is referred to as the critical plane. Therefore, the orientation of the crack nucleation path, θ_{cr}, is the one that satisfies the expression:

$$\overline{N}_{eq,a}(\theta_{cr}) = \max_{0° \le \theta \le 180°} \left\{ \overline{N}_{eq,a}(\theta) \right\} \tag{8}$$

Then, the position of the critical point P_{cr} where to perform the fretting fatigue assessment is assumed to be located at the end of the segment starting from H in the xz plane (shown in **Figure 3**), with length equal to $2L$ and direction defined by the angle θ_{cr}.

Finally, the fatigue life $N_{f,cal}$ is estimated through Eqs (4) and (5), by employing the values of the stress components acting on the critical plane at point P_{cr}: $N_a(\theta_{cr}, 2L)$, $N_m(\theta_{cr}, 2L)$ and $C_a(\theta_{cr}, 2L)$. Note that such values are computed by considering the critical plane

orientation as fixed (equal to θ_{cr}), that is, the procedure in Section 3.1 to determine the critical plane orientation through the off-angle δ is not applied here.

5. RESULTS AND DISCUSSION

In order to apply the proposed methodology to the experimental tests described in Section 2, the coefficient of friction between the contact surfaces is taken from the literature ($\mu = 0.72$). Details related to the experimental measurement of such a coefficient are provided in Ref.**[60]**. Since the fatigue material parameters had not been measured during the experimental campaign **[26, 42]**, the values of $\sigma_{af,-1}\left(N_0 = 1 \cdot 10^6\right)$ and m are derived from Ref. **[61]**: $169.15 MPa$ and -0.1553, respectively. Since experimental data related to S-N curve for torsion are not available in the literature, the following fatigue parameters are assumed in the case of torsion loading: $\tau_{af,-1}\left(N_0 = 1 \cdot 10^6\right) = \sigma_{af,-1}\left(N_0 = 1 \cdot 10^6\right) / \sqrt{3}$ and $m^* = m$. Moreover, the threshold stress-intensity factor range is taken equal to $\Delta K_{I,th} = 2.1 MPa\sqrt{m}$ (from Ref. **[62]**). Because such a value is related to loading ratio equal to zero, the fatigue limit range in Eq.(6), corresponding to the same loading ratio, is assumed to be equal to $\Delta\sigma_{af} = \Delta\sigma_{af,-1}/2 = 169.15 MPa$. Further, the value of the El-Haddad intrinsic crack length for Al 7075-T651 aluminium alloy can be computed through Eq.(6): $L = 0.0491 mm$.

For the loading configuration examined, the values of the contact semi-width a, the maximum Hertzian contact pressure p_0, the stick zone semi-width c, and the eccentricity e (that is, the shift of the stick zone induced by the cyclic bulk fatigue stress) are listed in **Table 3**.

Table 3.

Figures 5 (a), **(b)** and **(c)** show the estimated crack nucleation paths for loading configurations 1, 2 and 3, respectively. It can be observed that the estimated crack nucleation path turns towards the contact zone in all cases, with an inclination angle (measured from the line perpendicular to the contact surface) equal to $11°$, $10°$ and $9°$ for loading configurations 1, 2 and 3, respectively. For comparison, the experimental crack paths for tests Nos 1, 3 and 5 are also shown in **Figures 5 (a)**, **(b)** and **(c)**, respectively. It can be noted that the estimated crack paths agree quite well with those obtained from the experimental tests, with angular difference equal to 9°, 6° and 3° for tests Nos 1, 3 and 5, respectively.

Figure 5.

The analytical fatigue life is equal to $1134\,030$, $419\,667$ and $132\,184$ loading cycles for loading configurations 1, 2 and 3, respectively. The comparison between experimental and analytical fatigue life is shown in **Figure 6**, where the dashed lines

correspond to $N_{f,exp}/N_{f,cal}$ equal to 0.5 and 2. These lines define the scatter band 2.

Figure 6.

The same tests were analysed by Vázquez et al. [42] using a strain-based critical plane approach applied to a 3D finite element model. The analytical fatigue life was equal to 1017824, 294700 and 104212 loading cycles for loading configurations 1, 2 and 3, respectively. The comparison between experimental and numerical fatigue life is shown in **Figure 7.**

Figure 7.

The estimations obtained from these two different approaches can be considered quite satisfactory since all the results fall within scatter band 2.

The accuracy of the proposed fatigue life estimation can also be evaluated by means of the root mean square error method **[63],** where the mean square error T_{RMS} is given by:

$$T_{RMS} = 10^{E_{RMS}} \tag{9}$$

being E_{RMS} the value of the root mean square logarithmic error computed as follows:

$$E_{RMS} = \sqrt{\frac{\sum_{i=1}^{6} \log^2 \left(N_{f,exp}/N_{f,cal} \right)_i}{6}} \tag{10}$$

with i referring to the i-th test. In the present work, T_{RMS} is equal to 1.57, whereas $T_{RMS}=1$ means a perfect correlation between experimental and analytical values. The value of T_{RMS}, by taking into account the numerical results reported in Ref.**[42]**, is equal to 1.49.

In conclusion, the proposed methodology provides results (in terms of fretting fatigue life) characterised by an accuracy comparable with those related to different approaches **[42]**.

6. CONCLUSIONS

In the present paper, a new analytical methodology to estimate both crack path and lifetime of metallic structural components under fretting fatigue elastic partial slip loading condition has been proposed.

This methodology is based on the multiaxial fatigue criterion proposed by Carpinteri et al. **[43-45]** in the case of high-cycle fatigue regime. The fatigue life is evaluated by using an equivalent stress amplitude after reduction of the multiaxial stress state to an equivalent uniaxial one. The orientation of the critical plane is determined through the critical direction method by Araújo et al. **[46]**. In more detail, the critical plane is assumed to be the one that maximizes the averaged amplitude of the equivalent normal stress. Moreover, the critical distance method by Taylor **[47]**, in the form of the Line Method, is herein employed

in order to define the position of the critical point P_{cr} where to perform the fretting fatigue assessment.

Experimental and numerical tests carried out by Vázquez et al. **[26,42]** using two cylindrical fretting pads pushed against a dog-bone specimen, all these components being made of Al 7075-T651 aluminium alloy, have been exploited to evaluate the accuracy of the proposed methodology. More precisely, it can be noted that the estimated crack paths turn towards the contact zone in all cases examined, reproducing the experimental crack paths with a good agreement. Further, fretting fatigue life has satisfactorily been evaluated since all the results fall within scatter band 2.

Note that the proposed methodology avoids two drawbacks: (i) the need to evaluate the critical plane orientation in many points of the specimen, and (ii) anomalous situations occurring when the critical plane orientations determined in adjacent points may be completely different from each other.

In conclusion, the proposed methodology seems to be a promising tool to analyse the fretting fatigue phenomenon, but further investigations on different materials and contact configurations are needed.

Acknowledgements

The authors gratefully acknowledge the financial support provided by the Italian Ministry for University and Technological and Scientific Research (MIUR), Research Grant PRIN 2015 No. 2015JW9NJT on "Advanced mechanical modeling of new materials and structures for the solution of 2020 Horizon challenges".

REFERENCES

[1] Szolwinski MP, Farris TN. Mechanics of fretting fatigue crack formation. *Int J Fatigue*. 1997;19:39-49.

[2] Waterhouse RB. *Fretting corrosion*. UK: Pergamon; 1972.

[3] Waterhouse RB. Fretting fatigue. *Int Mater Rev*. 1992;37:77-97.

[4] Farrahi GH, Majzoubi GH. Crack behavior of the aluminum alloy 2024 under fretting conditions. *Int J Eng*. 2002;15:287-292.

[5] Hurricks PL. Mechanism of fretting. *Wear*. 1970;15:389-409.

[6] Berthier Y, Vincent L, Godet M. Fretting fatigue and fretting wear. *Tribol Int*. 1989;22:235-242.

[7] Endo K, Goto H. Initiation and propagation of fretting fatigue cracks. *Wear*. 1976;38:311-324.

[8] Hills DA, Nowell D, O'Connor J J. On the mechanics of fretting fatigue. *Wear*. 1988;125:129-146.

[9] Nishioka K, Hirakawa K. Fundamental investigations of fretting fatigue, part 3. *Bull Jpn Soc Mech Eng*. 1969;12:397-407.

[10] Chen JJ, Liu L, Li SX, Yu SR, He YN. Experimental and numerical investigation on crack initiation of fretting fatigue of dovetail. *Fatigue Fract Eng Mater Struct*. 2018;41:1426-1436.

[11] Minaii K, Farrahi GH, Karimpour M, Bahai H, Majzoobi GH. Investigation of microstructure effect on fretting fatigue crack initiation using crystal plasticity. *Fatigue Fract Eng Mater Struct*. 2019;42:640-650.

[12] Nesládek M, Španiel M, Kuželka J, Jurenka J, Doubrava K. A fretting damage correction factor applicable to the McDiarmid criterion of plain high-cycle fatigue. *Fatigue Fract Eng Mater Struct*. 2017;40:27-44.

[13] Yang Q, Zhou W, Gai P, Zhang X, Fu X, Chen G, Li Z. Investigation on the fretting fatigue behaviors of Ti-6Al-4V dovetail joint specimens treated with shot-peening. *Wear*. 2017;372-373:81-90.

[14] Chung CS, Kim HK. Fatigue strength of self-piercing riveted joints in lap-shear specimens of aluminium and steel sheets. *Fatigue Fract Eng Mater Struct*. 2016;39:1105-1114.

[15] Juoksukangas J, Lehtovaara A, Mäntylä A. Experimental and numerical investigation of fretting fatigue behavior in bolted joints. *Tribol Int*. 2016;103:440-448.

[16] Moraes JFC, Rao1 HM, Jordon JB, Barkey ME. High cycle fatigue mechanisms of aluminum self-piercing riveted joints. *Fatigue Fract Eng Mater Struct*. 2018;41:57-70.

[17] Hoeppner DW. Fretting fatigue case studies of engineering components. *Tribol Int.* 2006;39:1271–1276.

[18] Araújo JA, Castro FC, Pommier S, Bellecave J, Meriaux J. On the design and test of equivalent configurations for notch and fretting fatigue. *Fatigue Fract Eng Mater Struct*. 2016;39:1241–1250.

[19] Fadel AA, Rosa D, Murça LB, Fereira JLA, Araújo JA. Effect of high mean tensile stress on the fretting fatigue life of an Ibis steel reinforced aluminium conductor. *Int J Fatigue*. 2012;42:24–34.

[20] Sunde S.L., Berto F., Haugen B., Predicting fretting fatigue in engineering design, International Journal of Fatigue 117 (2018) 314–326.

[21] Anjum Z, Qayyum F, Khushnood S, Ahmed S, Shah M. Prediction of non-propagating fretting fatigue cracks in Ti6Al4V sheet tested under pin-in-dovetail configuration: experimentation and numerical simulation. *Mater Des*. 2015;87:750-758.

[22] Erena D, Vázquez J, Navarro C, Domínguez J. Voids as stress relievers and a palliative in fretting. *Fatigue Fract Eng Mater Struct*. 2018;41:2475–2484.

[23] Li X, Yang JW, Li MH, Zuo Z. An investigation on fretting fatigue mechanism under complex cyclic loading conditions. *Int J Fatigue*. 2016;88:227-235.

[24] Navarro C, Vázquez J, Domínguez J. A general model to estimate life in notches and fretting fatigue. *Eng Fract Mech*. 2011;78(8):1590-1601.

[25] Proudhon H, Fouvry S, Yantio GR. Determination and prediction of the fretting crack initiation: introduction of the (P, Q, N)

representation and definition of a variable process volume. *Int J Fatigue*. 2008;28:707-713.

[26] Vázquez J, Navarro C, Domínguez J. Analysis of fretting fatigue initial crack path in Al7075-T651 using cylindrical contact. *Tribol Int*. 2017;108:87-94.

[27] Walvekar AA, Leonard BD, Sadeghi F, Jalalahmadi B, Bolander N. An experimental study and fatigue damage model for fretting fatigue. *Tribol Int*. 2014;79:183-196.

[28] Bhatti NA, Wahab MA. Fretting fatigue crack nucleation: A review. *Tribol Int*. 2018;121:121-138.

[29] Walvekar AA, Leonard BD, Sadeghi F, Jalalahmadi B, Bolander N. An experimental study and fatigue damage model for fretting fatigue. *Tribol Int*. 2014;79:183-196.

[30] McDiarmid DL. A general criterion for high cycle multiaxial fatigue failure. *Fatigue Fract Eng Mater Struct*. 1991;14:429–53.

[31] Brown MW, Miller KJ. A theory for fatigue under multiaxial stress-strain conditions. In: *A Theory for Fatigue Under Multiaxial Stress-Strain Conditions, Proceedings of the Institute of Mechanical Engineers*; 1973:745–56.

[32] Fatemi A, Socie DF. A critical plane approach to multiaxial fatigue damage including out-of-phase loading. *Fatigue Fract Eng Mater Struct*. 1988;11:149–65.

[33] Smith K, Topper T, Watson P. A stress-strain function for the fatigue of metals. *J Mater*. 1970;5:767–78.

[34] Liu KC. A method based on virtual strain-energy parameters for multiaxial fatigue life prediction. In: McDowell DL, Ellis R, eds. *Advances in Multiaxial Fatigue*. Philadelphia: American Society for Testing and Materials; 1993:67–84.

[35] Crossland B. Effect of large hydrostatic pressures on the torsional fatigue strength of an alloy steel. In: *Proceedings of International Conference on Fatigue of Metals*; 1956:138–49.

[36] Ruiz C, Boddington PHB, Chen KC. An investigation of fatigue and fretting in a dovetail joint. *Exp Mech*. 1984;24:208–17.

[37] Ding J, Houghton D, Williams E, Leen S. Simple parameters to predict effect of surface damage on fretting fatigue. *Int J Fatigue*. 2011;33:332–42.

[38] Lemaitre J, Desmorat R. *Engineering damage mechanics: ductile, creep, fatigue and brittle failures*. Springer Science & Business Media; 2005.

[39] Bhattacharya B, Ellingwood B. Continuum damage mechanics analysis of fatigue crack initiation. *Int J Fatigue*. 1998;20:631–9.

[40] Chaboche JL, Lesne PM. A non-linear continuous fatigue damage model. *Fatig Fract Eng Mater Struct*. 1988;11:1–17.

[41] Lemaitre J. A continuous damage mechanics model for ductile fracture. *Transac ASME J Eng Mater Technol*. 1985;107:83–9.

[42] Vázquez J, Navarro C, Domínguez J. Two dimensional versus three dimensional modelling in fretting fatigue life prediction. *J Strain Analysis*. 2016;51:109-117.

[43] Carpinteri A, Spagnoli A, Vantadori S. Multiaxial fatigue assessment using a simplified critical plane-based criterion. *Int J Fatigue*. 2011;33:969–976.

[44] Carpinteri A, Ronchei C, Scorza D, Vantadori S. Critical plane orientation influence on multiaxial high-cycle fatigue assessment. *Phys Mesomech*. 2015;18:348–354.

[45] Ronchei C, Carpinteri A, Fortese G, Scorza D, Vantadori S. Fretting high-cycle fatigue assessment through a multiaxial critical plane-based criterion in conjunction with the Taylor's point method. *Solid State Phenomena*. 2016;258:217-220.

[46] Araújo JA, Almeida GMJ, Ferreira JLA, da Silva CRM, Castro FC. Early cracking orientation under high stress gradient: the fretting case. *Int J Fatigue*. 2017;100:302-311.

[47] Taylor D. *The theory of critical distances: a new perspective in fracture mechanics*. UK: Elsevier; 2007.

[48] Boller C, Seeger T. *Materials data for cyclic loading*. Elsevier Publishing Company; 1998.

[49] Navarro C, Vázquez J, Domínguez J. Nucleation and early crack path in fretting fatigue. *Int J Fatigue*. 2017;100:602–610.

[50] Johnson KL. *Contact mechanics*. UK: Cambridge University Press; 1985.

[51] Hertz H. Miscellaneous paper by Heinrich Hertz. Macmillan & Co., New York; 1896.

[52] Cattaneo C. Sul contatto di due corpi elastici: distribuzione locale degli sforzi. *Rendiconti dell'Accademia nazionale dei Lincei* 1938;27: 342-348.

[53] Mindlin RD. Compliance of elastic bodies in contact. *J Appl Mech*. 1949;16:259–268.

[54] McEwen E. Stress in elastic cylinders in contact along a generatrix. Phil Mag. 1949;40:454.

[55] Nowell D., Hills D.A. Mechanics of fretting fatigue tests. *Int J Mech Sci* 1987;29:355–65.

[56] Vantadori S., Fortese G., Ronchei C., Scorza D. A stress gradient approach for fretting fatigue assessment of metallic structural components. *International Journal of Fatigue* 2017;101:1 –8.

[57] Araújo JA, Carpinteri A, Ronchei C, Spagnoli A, Vantadori S. An alternative definition of the shear stress amplitude based on the maximum rectangular hull method and application to the C-S (Carpinteri-Spagnoli) criterion. *Fatigue Fract Eng Mater Struct*. 2014;37:764–771.

[58] Goodman J. *Mechanics Applied to Engineering*. UK: Longman, Green & Company; 1899.

[59] Araújo JA, Nowell D. The effect of rapidly varying contact stress fields on fretting fatigue. *Int J Fatigue*. 2002;24:763-775.

[60] Martín V., Navarro C., Vázquez J., Domínguez J. Mejora de la resistencia a fatiga por fretting con el tratamiento de shot peening. *Anales de Mecánica de la Fractura* 2017;34:82-88.

[61] Navarro C, Muñoz S, Domínguez J. Fracture mechanics approach to fretting fatigue behaviour of coated aluminium alloy components. *J Strain Anal Eng*. 2014;49:66–75.

[62] Navarro C, Vázquez J, Domínguez J. 3D vs. 2D fatigue crack initiation and propagation in notched plates. *Int. J. Fatigue*. 2014;58:40-46.

[63] Łagoda T, Walat K. Lifetime of semi-ductile materials through the critical plane approach. Int J Fatigue 2014;67:73–7.

Special issue on Advances in Fatigue and Fracture

celebrating the 40th anniversary of FFEMS

March 2019

Lifetime estimation of mechanical assemblies under constant amplitude fretting fatigue loading

Andrea Carpinteri, Sabrina Vantadori, Andrea Zanichelli

Department of Engineering & Architecture, University of Parma,

Parco Area delle Scienze 181/A, 43124 Parma, Italy

Corresponding Author:

Andrea Carpinteri, andrea.carpinteri@unipr.it

FIGURES AND TABLES

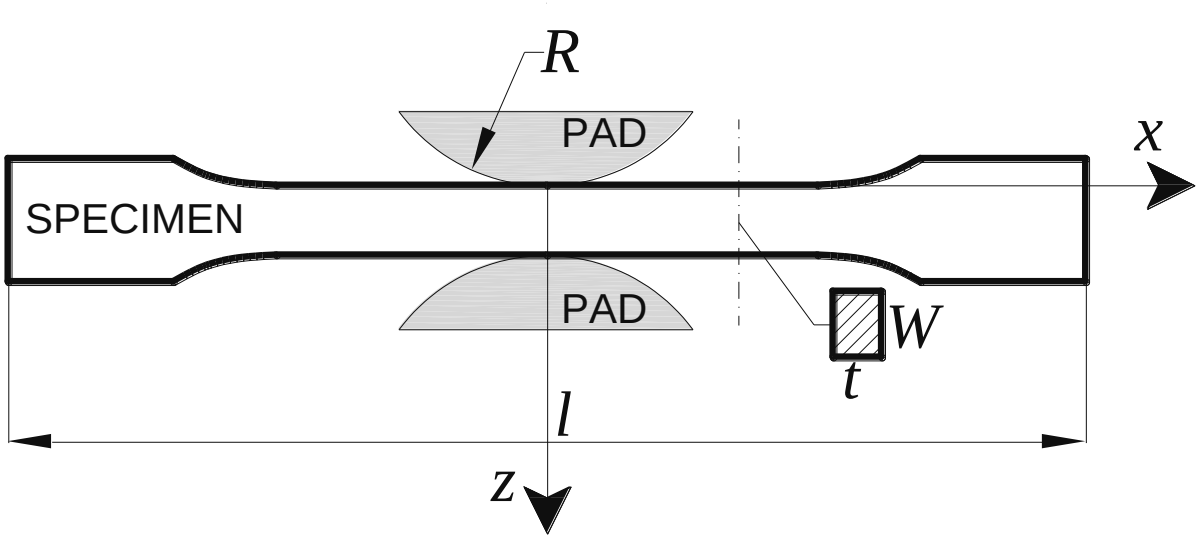

Figure 1. Experimental setup in the fretting fatigue tests: test specimen and pads.

Table 1. Mechanical properties for the Al 7075-T651 alloy **[48].**

Young's modulus	E	71000 MPa
Poisson's coefficient	ν	0.33
Yield strength	σ_y	503 MPa
Ultimate tensile strength	σ_u	572 MPa

Table 2. Fretting fatigue loads and experimental fatigue life values, for each test examined **[42].** The subscript a stands for amplitude.

LOADING CONFIGURATION No.	TEST No.	P [N]	Q_a/P	$\sigma_{B,a}$ [MPa]	$N_{f,exp}$ [cycles]
1	1	5800	0.15	50	676704
1	2	5800	0.15	50	577540
2	3	5800	0.19	55	283110
2	4	5800	0.19	55	252878
3	5	5800	0.23	70	167324
3	6	5800	0.23	70	165421

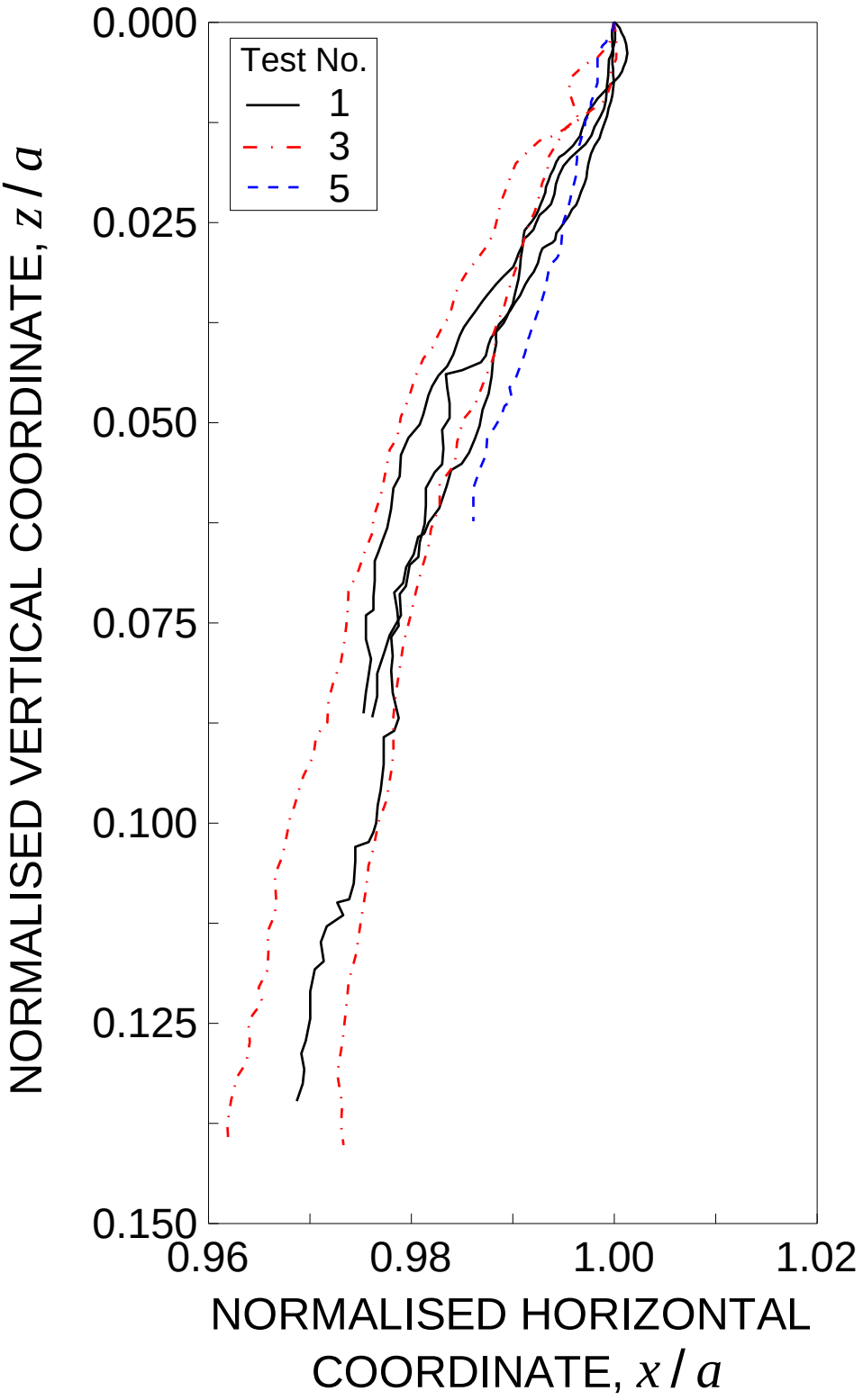

Figure 2. Experimentally observed crack paths for tests Nos 1, 3 and 5 **[49]**.

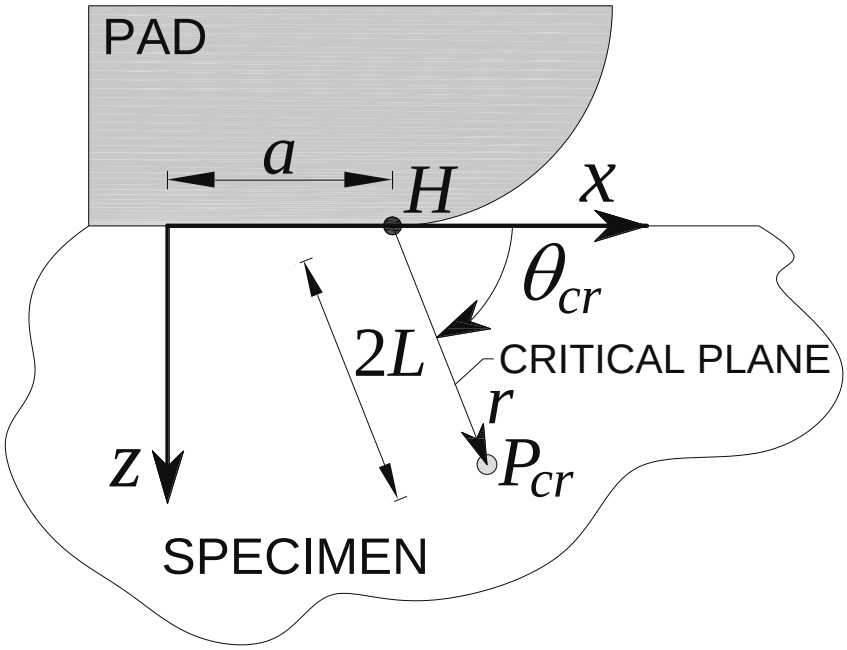

Figure 3. Schematization of the procedure to determine the critical point P_{cr}.

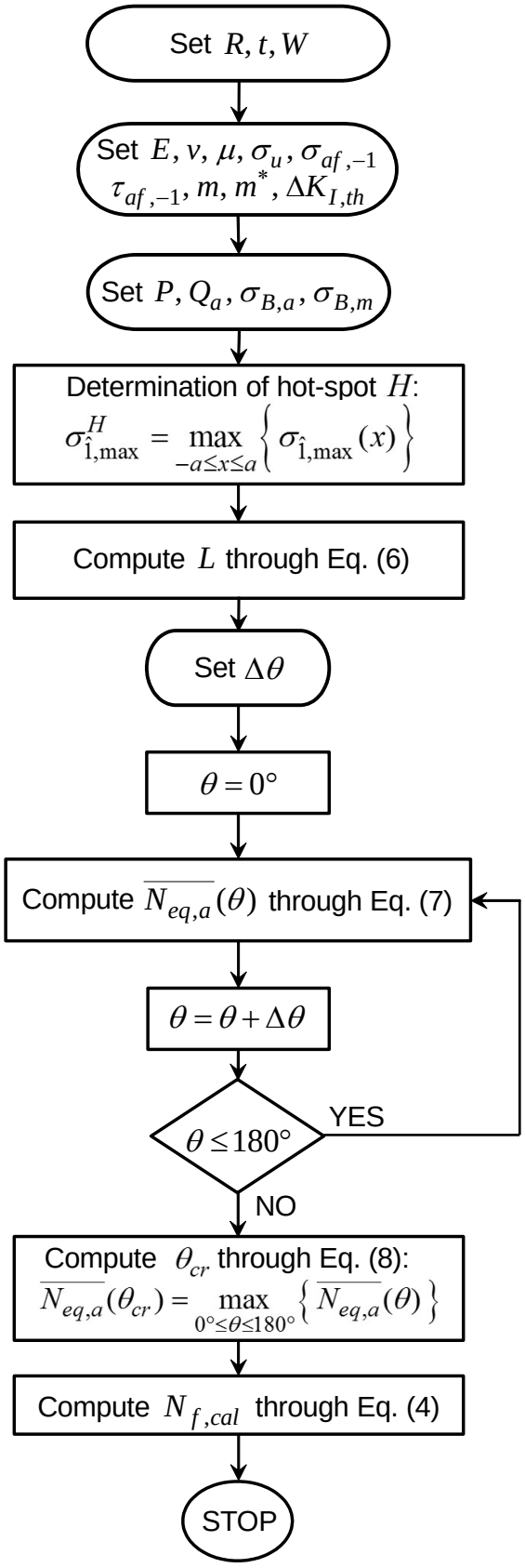

Figure 4. Flowchart of the proposed methodology.

Table 3. Contact parameters for each fretting fatigue loading configuration examined.

LOADING CONFIGURATION No.	a [mm]	p_0 [MPa]	c [mm]	e [mm]
1	1.627	324.21	1.448	0.087
2	1.627	324.21	1.396	0.096
3	1.627	324.21	1.342	0.122

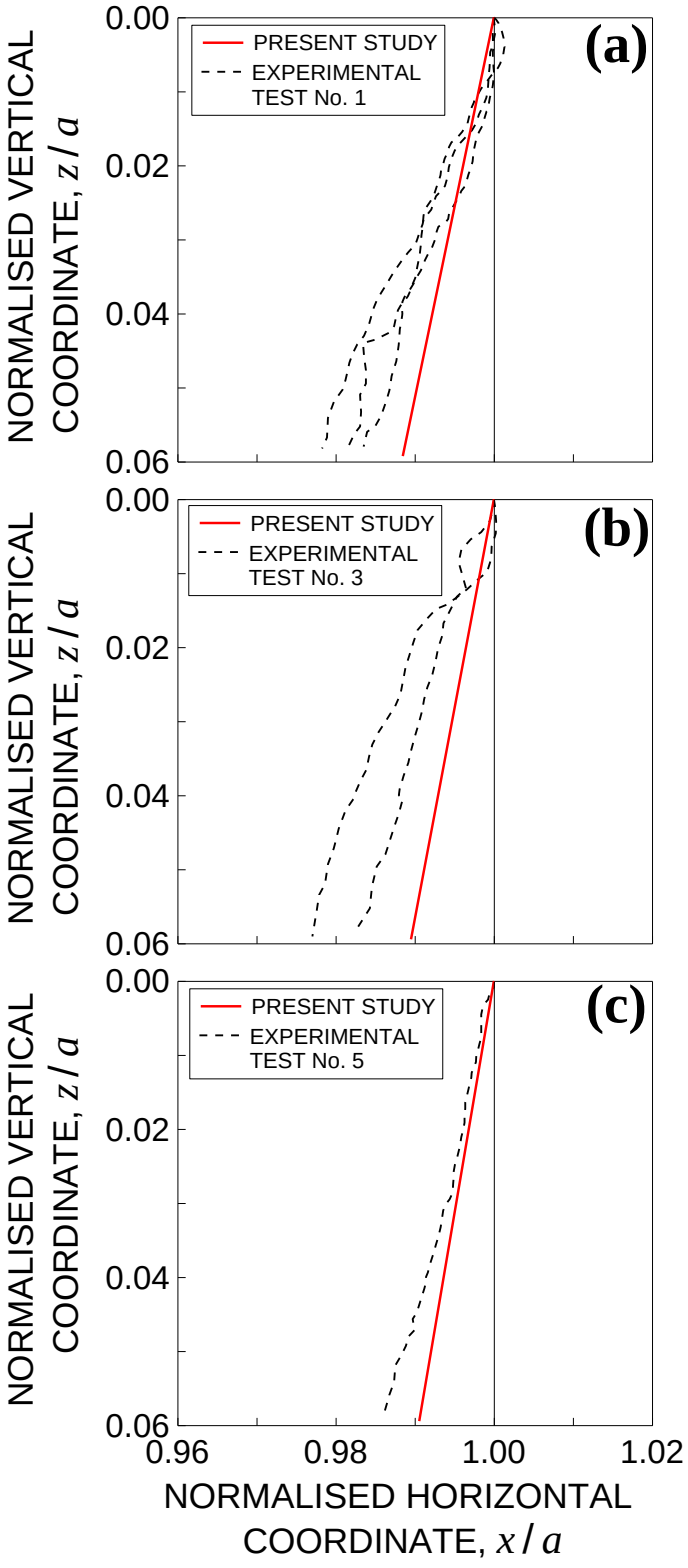

Figure 5. Analytically predicted crack paths for loading configurations 1, 2 and 3, respectively (see (a),(b) and (c)). The experimental crack paths are also plotted for comparison.

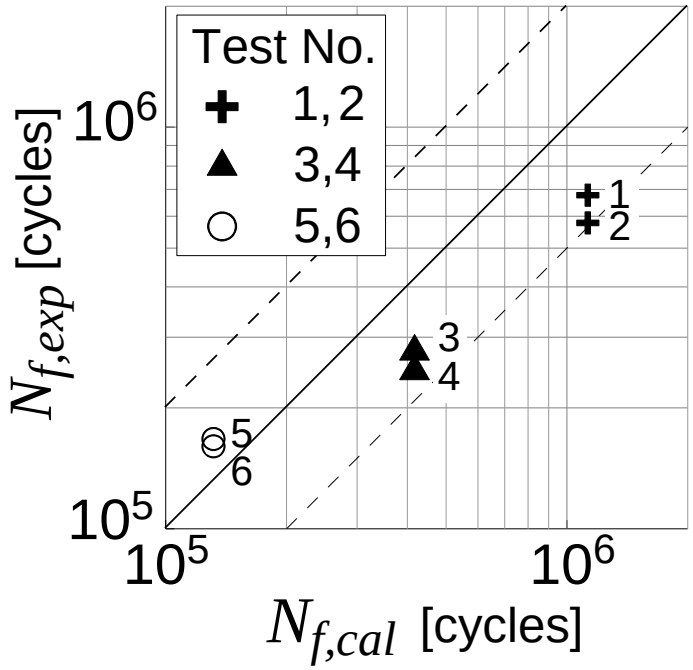

Figure 6. Comparison between experimental and analytical fatigue life. The numbers are related to the test numbers (see Table 2).

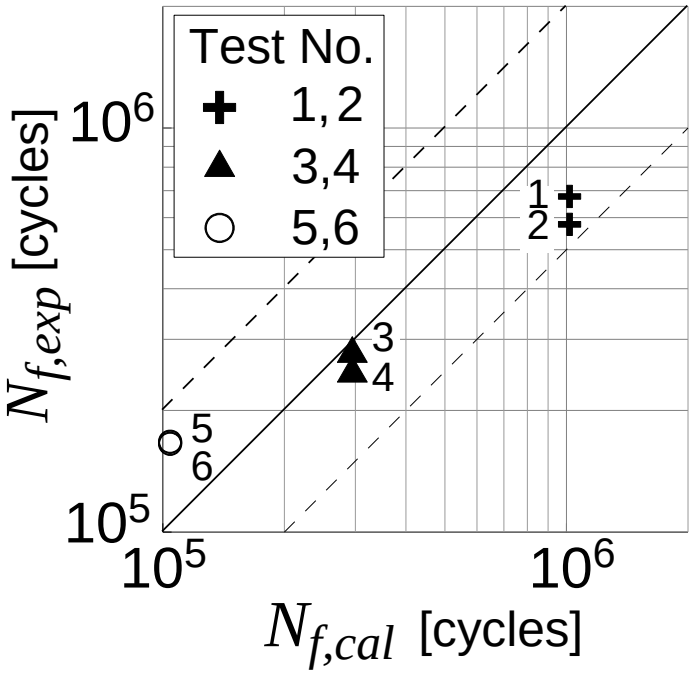

Figure 7. Comparison between experimental and numerical fatigue life, both reported in Ref.**[42]**. The numbers are related to the test numbers (see Table 2).